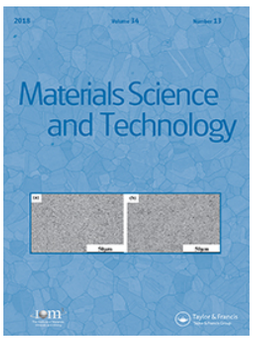

Materials Science and Technology

ISSN: 0267-0836 (Print) 1743-2847 (Online) Journal homepage: http://www.tandfonline.com/loi/ymst20

Characterisation of secondary phases in Ni-base superalloy Rene 65

Tomasz Wojcik, Markus Rath & Ernst Kozeschnik

To cite this article: Tomasz Wojcik, Markus Rath & Ernst Kozeschnik (2018) Characterisation of secondary phases in Ni-base superalloy Rene 65, Materials Science and Technology, 34:13, 1558-1564, DOI: 10.1080/02670836.2018.1505227

To link to this article: https://doi.org/10.1080/02670836.2018.1505227

Published online: 09 Aug 2018.

MATERIALS SCIENCE AND TECHNOLOGY
2018, VOL. 34, NO. 13, 1558–1564
https://doi.org/10.1080/02670836.2018.1505227

The Institute of Materials, Minerals and Mining

Taylor & Francis
Taylor & Francis Group

Characterisation of secondary phases in Ni-base superalloy Rene 65

Tomasz Wojcik, Markus Rath and Ernst Kozeschnik

Institute for Materials Science and Technology, TU Wien, Wien, Austria

ABSTRACT

The Ni-base superalloy Rene 65 is a newly introduced cast and wrought alloy, used for turbine disc applications in aero-engines. The fine-grained and γ'-strengthened alloy was developed to increase service temperatures up to over 700°C and therefore, enhance the efficiency of aerospace turbines.

In this work, the phases occurring in the as-received material as well as after continuous cooling experiments are characterised by transmission electron microscopy (TEM). In the as-received material, a tri-modal γ' size distribution is found, ranging from a few nanometres up to approx. 5 µm. In addition, borides are found preferentially at grain boundaries with a size of approx. 1 µm. For different cooling rates, a change in morphology and size distribution of γ' precipitates is found.

ARTICLE HISTORY
Received 28 February 2018
Revised 7 July 2018
Accepted 22 July 2018

KEYWORDS
Rene 65; superalloys; cast and wrought; turbine discs; gamma prime; TEM

This is part of a thematic issue on Nanoscale Materials Characterisation and Modeling by Advances Microscopy Methods - EUROMAT.

Introduction

The main objectives for developing new alloys for aero-engines applications are high strength, long-term stability of the microstructure and corrosion resistance at elevated temperatures and high pressures. A wide range of Ni-base superalloys meets these requirements. Most of them exhibit an fcc γ-matrix with fine dispersed coherent γ' precipitates, forming an ordered $L1_2$ crystal structure of $Ni_3(Ti,Al)$ type, or other Ni_3X compounds, like e.g. the γ"-phase in the Inconel 718 alloy [1].

The recently developed Ni-base superalloy Rene 65 has been designed by General Electrics typically for turbine disc applications in aero-engines. One of the main design objectives was to increase the service temperature up to over 700°C, and therefore, enhance the efficiency of aerospace turbines. This aim is achieved by the forming of more stable γ' precipitates than γ", which occur in the currently used alloys like Inconel 718 and are prone to dissolve at higher temperatures [2,3]. In contrast to the powder metallurgical alloys like IN100, Rene 65 is produced by the less cost-intensive triple melting technology which consists of Vacuum Induction Melting (VIM), followed by Electroslag Remelting (ESR) and Vacuum Arc Remelting (VAR) [4]. The Rene 65 is a fine-grained and γ'-strengthened alloy which is processed by the cast and wrought route. The chemical composition (see Table 1) is derived from the Rene 88DT alloy. In comparison to Rene 88DT, another advantage of Rene 65 is its forgeability in a conventional hot die forging routine [5].

Industrially applied complex heat treatments lead to multimodal size distributions of γ' precipitates, reaching high number densities and volume fractions up to 60% [6]. Large primary γ' precipitates pin the grain boundaries and thus stabilise the microstructure, the fine dispersed secondary and tertiary γ' precipitates are responsible for the high strength of the material [7]. Therefore, the knowledge of the precipitation kinetics and the control of the precipitate evolution are crucial for ensuring the optimal mechanical properties for turbine disc applications.

It is well known that precipitation occurs in three stages: nucleation, growth and coarsening [8]. Since precipitation is a diffusion-controlled process, the nucleation and growth mechanisms are strongly dependent on the temperature evolving during continuously cooling. The nucleation and growth of tertiary γ' precipitates can be explained by the competition between increasing supersaturation due to continuous cooling and decreasing supersaturation due to the formation of secondary γ' precipitates in the matrix [7]. The precipitation of γ' particles in the matrix results in an elemental partitioning – a local depletion of γ' forming elements in the γ-matrix around the precipitates [9–11]. Decreasing temperature reduces the growth of the secondary precipitates due to decreasing diffusivity. With further undercooling, the matrix supersaturates with γ' forming elements, until a new population of tertiary precipitates starts to nucleate between the secondary γ' precipitates [7,12–14].

CONTACT Tomasz Wojcik tomasz.wojcik@tuwien.ac.at Institute for Materials Science and Technology, TU Wien, Getreidemarkt 9, 1060 Wien, Austria

Table 1. Chemical composition of the Rene 65 alloy.

Ni	Cr	Mo	W	Co	Fe	Nb	Ti	Al	Zr	B
Bal	16	4	4	13	1	0.7	3.7	2.1	0.05	0.016

Note: Major elements, weight per cent.

Depending on the heat treatment and the γ/γ' lattice mismatch, the morphology of the secondary γ' precipitates evolves from initially spheres, over cubes and octo-cubes to more complex structures. Higher lattice mismatches lead to a faster coherency loss and a transition to more complex structures during heat treatments. Slower cooling rates or isothermal heat treatments at high temperatures lead to more complex structures [1,6,7,10,15–17].

Besides of the γ' precipitates also other precipitate phases are expected in the Rene 65 alloy, such as borides, titanium nitrides, or topologically closed packed (TCP) phases. The addition of a small amount of boron improves the high-temperature mechanical properties. Boron segregates to the grain boundaries, retarding the formation of carbides there. Excess boron forms borides with Mo, Ti, Cr and Ni, which are as well as carbides, nitrides and TCP phases reported to be deleterious to the alloys due to their brittleness [1,2,18–20].

The aim of this work is to characterise the phases present in the as-received material condition as well as in heat-treated conditions after continuous cooling experiments, using transmission electron microscopy (TEM). By evaluating the results, the phase stabilities of the occurring precipitates can be determined. According to the experimental results for the Rene 88DT alloy published by Wlodek et al. [16] and Mao et al. [21], we expect a multimodal size distribution for the γ' precipitates for slow cooling rates only, and a unimodal distribution for high cooling rates. In a follow-up publication, we will compare the experimental results of this work with thermo-kinetic precipitation simulations, employing the CALPHAD-based software package MatCalc [22].

Experimental

The samples for continuous cooling experiments were machined from the mid-radius position of the as-received billet disc material. The nearly cylindrical shape of the samples had a diameter of approx. 5 mm and a length of 10 mm. The heat treatments were carried out on the dilatometer Bähr DIL 805 A/D, where the samples were heated up inductively in a vacuum and cooled by He gas. The process temperature was controlled by S-type thermocouples. In order to ensure the same condition for all experiments, the as-received material was heated up and solution annealed at 1150°C for 1 h first. At this point all γ'precipitates are dissolved and the alloying elements homogenously distributed in

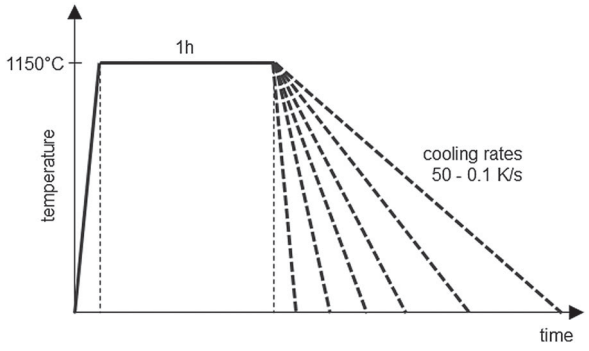

Figure 1. Continuous cooling experiments. After solution annealing at 1150°C for 1 h, the samples are cooled down to room temperature at constant cooling rates from 0.1 to 50 K s^{-1}.

the γ-matrix. Subsequently, the samples were cooled down to room temperature at constant cooling rates ranging from 0.1 up to 50 K s^{-1}. A schematic graph of the heat treatments is shown in Figure 1.

In order to analyse the as-received condition as well as the evolution of γ' precipitates depending on the cooling rate in TEM, thin foils were prepared. The samples were cut and ground down to a thickness of approx. 0.1 mm. After punching out discs with a diameter of 3 mm, they were electrochemically etched on a Struers Tenupol 5, using a 7% solution of a perchloric acid at temperatures around −10°C. The investigation of the samples was performed on the transmission electron microscope FEI Tecnai F20, equipped with a field emission gun and operated at 200 kV. The chemical composition of metallic phases was analysed by means of energy dispersive x-ray spectroscopy (EDX). In the detected boride phases, the EDX-quantification was combined with the results of electron energy loss spectroscopy (EELS) because of the weak x-ray yield of boron. In the EEL spectra, the ratio of B and Cr was estimated upon the K-edges of these elements and combined with EDX results. The crystal structures were determined using selected area electron diffraction (SAED). Based on the results on the chemically similar Rene 88DT alloy [16], two tetragonal crystal structures for the borides were taken into account: M_3B_2 with lattice constants of $a = b = 0.5787$ nm and $c = 0.3123$ nm and an M_5B_3 phase with $a = b = 0.572$ nm and $c = 1.08$ nm. The imaging of the γ' precipitates were achieved in two modes: TEM dark field mode and scanning TEM mode with a high angle annular dark field detector (STEM-HAADF). Since the γ-matrix and the coherent γ' precipitates form the same fcc crystal structure with a lattice constant mismatch below 1%, the $L1_2$ ordered γ' phase shows $<001>$ diffraction reflections which do not occur in the disordered γ-matrix due to a systematic absence. This allows the visualisation of the γ' precipitates in dark field TEM mode on $<001>$ diffraction spots. In STEM-HAADF mode a fine electron

probe is scanning over a defined sample area and the contrast is dependent on the mass of each illuminated point. Heavier elements and thicker regions appear bright, light elements and thin regions dark. Area fractions of secondary γ' precipitates, being equal to volume fractions, were calculated from estimated mean particle diameters, by counting the number of precipitates detected in a defined area, under the assumption that the sample is thin enough, not to count overlapping particles.

Results and discussion

The microstructure of the as-received material exhibits a multimodal precipitation distribution. In the representative STEM-HAADF micrograph in Figure 2, fine dispersed secondary γ' precipitates with sizes of about 200 nm are dense distributed in the matrix. Besides them a primary γ' precipitate with a diameter of approx. 3 µm is detected on a grain boundary. The purpose of the primary precipitates is the grain size control during heat treatments. One of the two approx. 1.5 µm large particles in the grain was indexed as M_3B_2 boride in the [100] zone axis by means of SAED (see diffraction pattern in Figure 2). The chemical composition of the borides was determined by acquiring EDX and EEL spectra. The combined quantification of these spectra in Table 2 shows a Cr- and Mo-rich boride with a metal to boron ratio of nearly 3:2, which matches the stoichiometry of the phase very good. A closer view in Figure 3 shows secondary octo-cube shaped γ' precipitates with sizes of approx. 200 nm. The quantification of an EDX spectrum obtained on one of these precipitates in Table 3, shows mainly the typical γ' formers like Ni, Ti and Al. Between the secondary γ' precipitates some tertiary precipitates are visible.

Applying solution annealing and subsequent cooling at different cooling rates, as shown in Figure 1, causes different size distributions and morphologies of γ' precipitates. Representative TEM dark field micrographs on the $<001>$ diffraction spot for the applied cooling rates are shown in Figure 4. As expected, the particle sizes decrease with increasing cooling rates. Starting at approx. 300 nm for 0.1 K s^{-1}, we end up at about 10 nm for 50 K s^{-1}. Such small precipitates are difficult to measure in TEM dark field micrographs because of the small volumes, compared to the massive matrix and therefore very weak contrast. Mao et al. presented a similar study on the Rene 88DT alloy [21] and derived an empirical formula from their results, showing the mean diameter of the precipitates as a linear function of the cooling rate in a double logarithmic scale. We compared the values of this formula with our results in

Table 2. Combined EDX and EELS quantification of a M_3B_2 boride in the as-received material in atomic per cent.

Ni	Cr	Mo	W	Co	Fe	Nb	Ti	Al	B
3.9	29.3	15.0	4.8	3.0	1.3	1.2	2.7	0.0	38.9

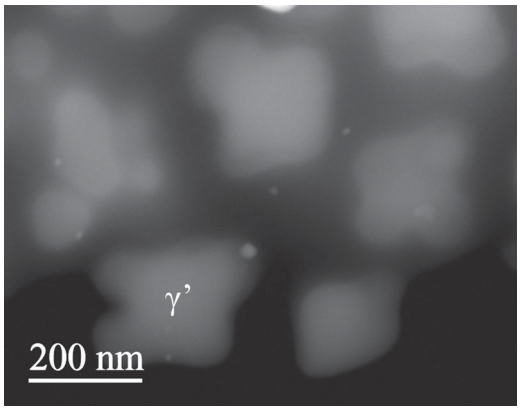

Figure 3. STEM-HAADF micrograph of the as-received material. Secondary γ' precipitates with diameters of $\sim$200 nm and tertiary γ' precipitates between them.

Table 3. EDX quantification of secondary γ' precipitates in the as-received material in atomic per cent.

Ni	Cr	Mo	W	Co	Fe	Nb	Ti	Al
68.5	2.6	0.7	0.3	6.4	0.7	0.6	12.0	8.3

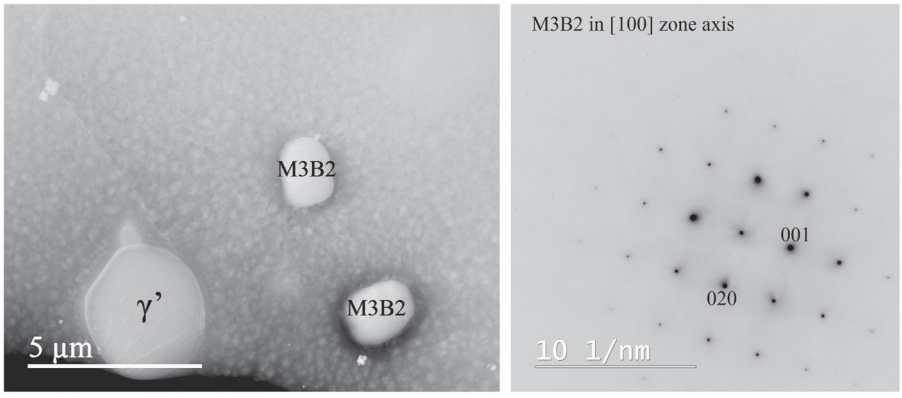

Figure 2. STEM-HAADF overview of the as-received material (left). Matrix with secondary γ' precipitates. Primary γ' precipitate with a diameter of 3 µm on a grain boundary, two borides with diameters of 1.5 µm. SAED pattern of a M_3B_2 boride in [100] zone axis (right).

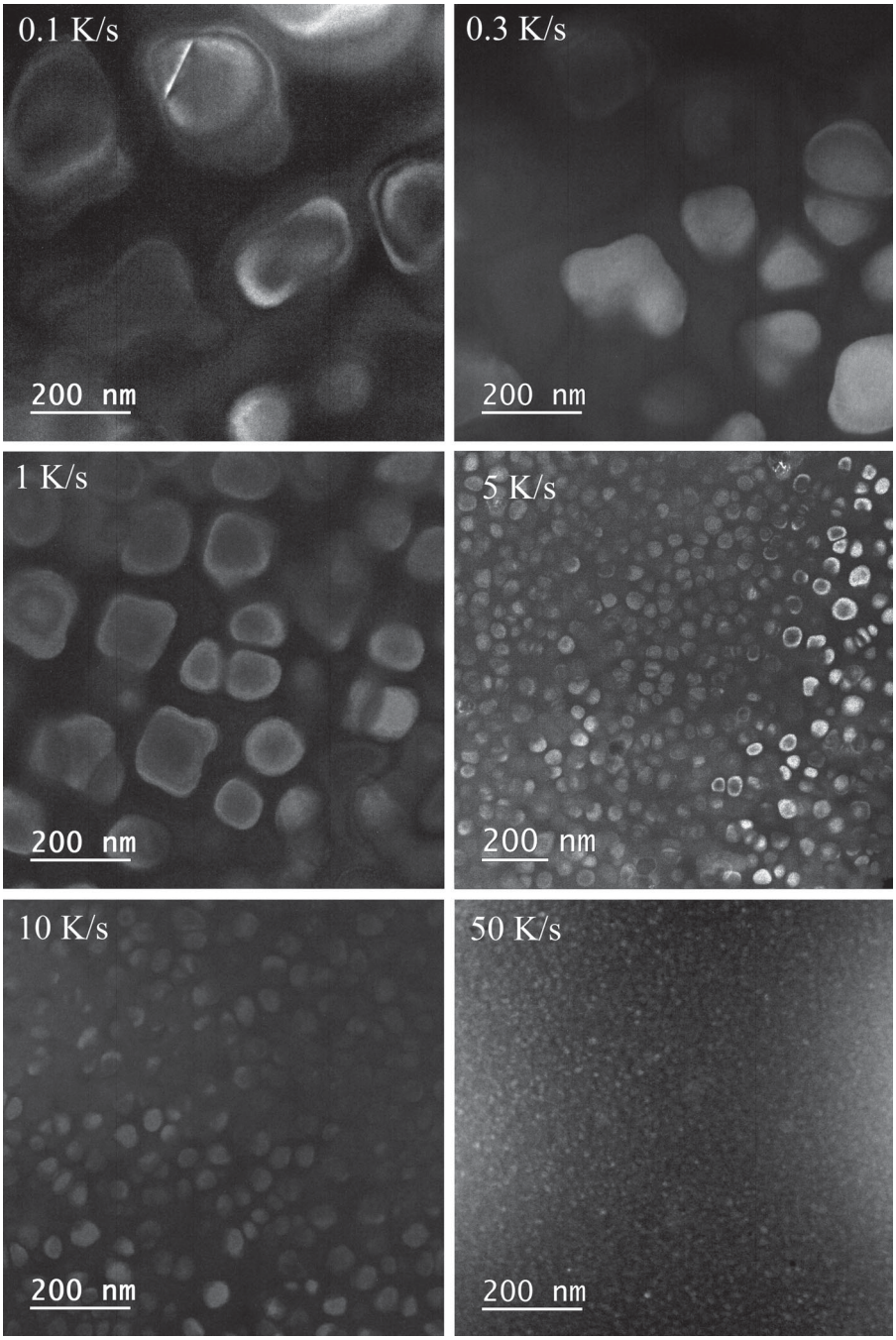

Figure 4. TEM dark field images on the $< 100 >$ diffraction reflection. Evolution of γ' precipitates depending on cooling rates ranging from 0.1 to 50 K s^{-1}.

Figure 5. Although we hit the linear trend in the graph, we measure lower particle sizes for a very similar alloy. As reason for this mismatch, we assume differences in the experimental setup and different volume fractions determined in both studies. While we measure volume fractions of 40% and above, Mao et al. report 27–36%. For the slow cooling rates of 0.1 and 0.3 K s^{-1}, we determined slightly lower volume fractions of the secondary γ' precipitates at 40% and 39%, respectively. In samples cooled faster at 1 –10 K s^{-1}, the corresponding volume fractions reach values of 44–45%. At slow cooling rates a part of γ' formers accounts for the forming of tertiary precipitates, which results in lower volume fractions of the secondary precipitates. Due to very weak contrast values, the measuring of tertiary precipitates in slowly cooled samples and the measuring of the secondary precipitates in samples cooled at a rate of 50 K s^{-1} seems not reliable. In Figure 6, tertiary γ' precipitates between the large secondary particles are shown in TEM bright field and dark field mode for the slowest cooling rates. While in the sample with 0.1 K s^{-1} (left) small tertiary precipitates are visible, in the right picture (0.3 K s^{-1}) it seems speculative if there are small tertiary precipitates directly after nucleation.

In addition, the evolution of particle morphologies for different cooling rates meets the expectations

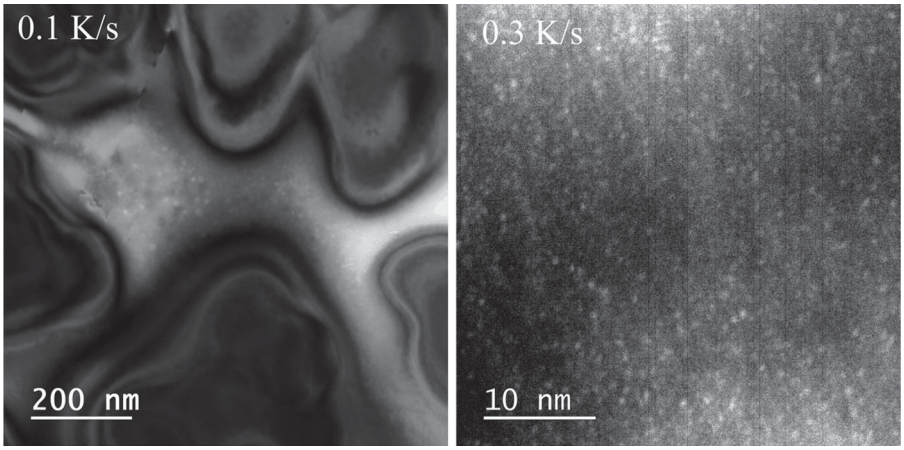

Figure 5. TEM bright field image of tertiary γ' precipitates at a cooling rate of 0.1 K s^{-1} with sizes of approx. 10 nm (left) and TEM dark field image at a cooling rate of 0.3 K s^{-1} with nucleating tertiary γ' precipitates (right).

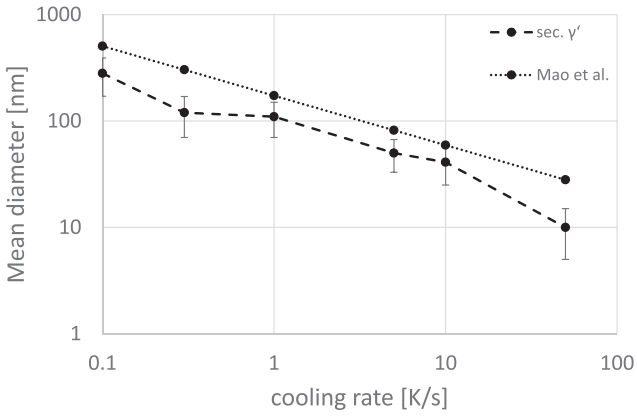

Figure 6. Mean size of secondary γ' precipitates as function of the cooling rate in comparison to the empirical formula values derived from a similar study on the Rene 88DT alloy by Mao et al. [21].

coming from former studies on similar alloys. While the slow-cooled samples exhibit complex and octocuboidal shapes, the secondary precipitates in samples with cooling rates of 5 and 10 K s^{-1} are cubes and spheres. The small precipitates in the sample cooled at a rate of 50 K s^{-1} are spherical.

Table 4. EDX quantification of a secondary γ'-precipitate compared to the matrix in a sample with a cooling rate of 0.1 K s^{-1} in atomic per cent.

	Ni	Cr	Mo	W	Co	Fe	Nb	Ti	Al
Matrix	48.3	26.8	3.3	0.8	16.3	1.7	0.3	1.4	1.2
Sec. γ'	70.8	2.5	0.3	0.3	6.9	0.8	0.5	11.8	6.1

A representative EDX-quantification of the matrix and a large γ' precipitate shown in Table 4 confirms the enrichment of γ'-formers Ni, Ti and Al in the precipitate and depletion of the other elements.

In all continuously cooled samples, we found borides preferable on grain boundaries. An elongated boride on a grain boundary is shown in the representative TEM bright field image in Figure 7. We chose this particle on the edge of the sample, in order to improve the quality of the chemical analysis, by decreasing the contribution of the surrounding. The indexing of the corresponding SAED pattern in Figure 7 shows a match with the M_5B_3 crystal structure in the [111] zone axis. In other samples, we also detected M_3B_2 borides on grain boundaries. The combined quantification of EDX

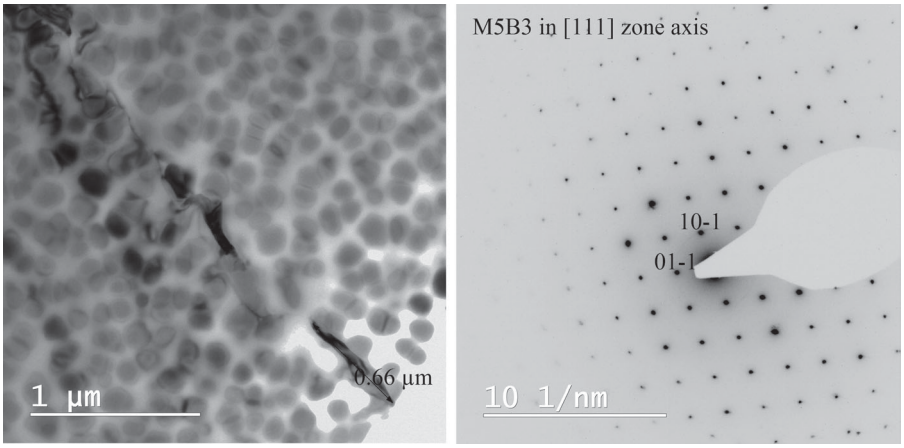

Figure 7. TEM bright field image of an elongated M_5B_3 particle in the [111] zone axis on a grain boundary with a length of approx. 0.66 µm (left) and the corresponding SAED pattern (right).

Table 5. Combined EDX and EELS quantification of a M_5B_3 boride in a sample cooled at a rate of 1 K s^{-1} in atomic per cent.

Ni	Cr	Mo	W	Co	Fe	Nb	Ti	Al	B
2.0	45.3	11.2	2.1	1.4	0.3	0.2	0.5	0.1	37.0

and EEL spectra on this particle in Table 5 shows a B-content of approx. 37 atomic per cent. This value is in good accordance with the stoichiometry of this phase. Since the borides occur in the as-received material, as well as in all continuous cooled samples, they are supposed not to dissolve during solution annealing. After the dissolution of the primary γ' precipitates the grains grow during solution annealing and the borides pin the grain boundaries.

Conclusions

- The microstructure of the as-received material reveals a tri-modal γ' precipitation with over 1 µm large primary, about 200 nm large secondary, and tertiary particles with sizes of approx. 10 nm. Additionally, Cr- and Mo-rich borides with tetragonal crystal structure larger than 1 µm were found.
- The results of continuous cooling experiments show decreasing precipitate sizes as a function of increasing cooling rates. A comparison with a study on a similar alloy [21] shows the same trend but smaller precipitates for all cooling rates. The discrepancy can be explained by higher volume fractions of precipitates in that study.
- Tertiary γ' precipitates were detected only in the samples with the slowest cooling rates of 0.1 and 0.3 K s^{-1}. This is the reason for the lower volume fractions of secondary precipitates of 39–40%, compared with values of 44–45% for faster-cooled samples, where no tertiary precipitates were detected.
- The particle morphologies are spherical for high cooling rates. With decreasing cooling rates, the shapes of the precipitates become first cuboidal and then more and more complex.
- Cr- and Mo-rich borides with sizes of approx. 1 µm occurred in all investigated samples preferably on grain boundaries. No TCP phases were observed.

Acknowledgements

The authors kindly acknowledge voestalpine BÖHLER Aerospace GmbH & Co KG for providing the material and specialist support. The TEM-investigation was carried out, using the facilities at the University Service Centre for Transmission Electron Microscopy, TU Wien, Austria. The authors acknowledge the TU Wien University Library for financial support through its Open Access Funding Program.

Disclosure statement

No potential conflict of interest was reported by the authors.

Funding

Financial support by the Austrian Federal Government (in particular from Bundesministerium für Verkehr, Innovation und Technologie and Bundesministerium für Wissenschaft, Forschung und Wirtschaft) represented by Österreichische Forschungsförderungsgesellschaft mbH and the Styrian and the Tyrolean Provincial Government, represented by Steirische Wirtschaftsförderungsgesellschaft mbH and Standortagentur Tirol, within the framework of the COMET Funding Programme is gratefully acknowledged.

References

[1] Jena AK, Chaturvedi MC. The role of alloying elements in the design of nickel-base superalloys. J Mater Sci. 1984;19:3121–3139.
[2] Laurence A, Cormier J, Villechaise P, et al. Impact of the solution cooling rate and of thermal aging on the creep properties of the new cast & wrought René 65 Ni-based superalloy. Proc. 8th Int. Symp. Superalloy 718 Deriv. Hoboken, NJ: John Wiley & Sons, Inc.; 2014. p. 333–348.
[3] Wessman A, Laurence A, Cormier J, et al. Thermal stability of cast and wrought alloy Rene 65. Superalloys 2016. Hoboken, NJ: John Wiley & Sons, Inc.; 2016. p. 793–800.
[4] Moyer JM, Jackman LA, Adasczik CB, et al. Advances in triple melting superalloys 718, 706 and 720. Superalloys 718, 625, 716 Deriv. PA: Pittsburgh; 1994. p. 39–48.
[5] Bond BJ, O'Brien CM, Russell JL, et al. René 65 Billet material for forged turbine components. Proc. 8th Int. Symp. Superalloy 718 Deriv. Hoboken, NJ: John Wiley & Sons, Inc.; 2014. p. 107–118.
[6] Ricks RA, Porter AJ, Ecob RC. The growth of γ' precipitates in nickel-base superalloys. Acta Metall. 1983;31:43–53.
[7] Radis R, Schaffer M, Albu M, et al. Evolution of size and morphology of γ' precipitates in UDIMET 720 Li during continuous cooling. Superalloys 2008 Eleventh Int. Symp. TMS. PA: Champion; 2008. p. 829–836.
[8] Svoboda J, Fischer FD, Fratzl P, et al. Modelling of kinetics in multi-component multi-phase systems with spherical precipitates I: theory. Mater Sci Eng A. 2004;385:166–174.
[9] Hwang JY, Banerjee R, Tiley J, et al. Nanoscale characterization of elemental partitioning between gamma and gamma prime phases in René 88 DT nickel-base superalloy. Metall Mater Trans A. 2009;40:24–35.
[10] Babu SS, Miller MK, Vitek JM, et al. Characterization of the microstructure evolution in a nickel base superalloy during continuous cooling conditions. Acta Mater. 2001;49:4149–4160.
[11] Hwang JY, Nag S, Singh ARP, et al. Compositional variations between different generations of γ' precipitates forming during continuous cooling of a commercial nickel-base superalloy. Metall Mater Trans A. 2009;40:3059–3068.
[12] Singh ARP, Nag S, Hwang JY, et al. Influence of cooling rate on the development of multiple generations of γ' precipitates in a commercial nickel base superalloy. Mater Charact. 2011;62:878–886.
[13] Singh ARP, Nag S, Chattopadhyay S, et al. Mechanisms related to different generations of γ' precipitation during continuous cooling of a nickel base superalloy. Acta Mater. 2013;61:280–293.

[14] Sarosi PM, Wang B, Simmons JP, et al. Formation of multimodal size distributions of γ' in a nickel-base superalloy during interrupted continuous cooling. Scr Mater. 2007;57:767–770.
[15] Tiley J, Viswanathan GB, Srinivasan R, et al. Coarsening kinetics of γ' precipitates in the commercial nickel base superalloy René 88 DT. Acta Mater. 2009;57:2538–2549.
[16] Wlodek ST, Kelly M, Alden DA. The structure of Rene' 88DT. Superalloys 1996; Eighth Int. Symp. TMS. Champion: PA; 1996. p. 129–136.
[17] Bhowal PR, Wright EF, Raymond EL. Effects of cooling rate and γ' morphology on creep and stress-rupture properties of a powder metallurgy superalloy. Metall Trans A. 1990;21:1709–1717.
[18] Xiao L, Chen DL, Chaturvedi MC. Effect of boron on the low-cycle fatigue behavior and deformation structure of INCONEL 718 at 650 °C. Metall Mater Trans A. 2004;35 A:3477–3487.
[19] Ojo OA, Zhang HR. Analytical electron microscopy study of boron-rich grain boundary microconstituent in directionally solidified RENE 80 superalloy. Metall Mater Trans A. 2008;39:2799–2803.
[20] Garosshen TJ, Tillman TD, Mccarthy GP. Effects of B, C, and Zr on the structure and properties of a P/M nickel base superalloy. Metall Trans A. 1987;18A: 69–77.
[21] Mao J, Chang KM, Yang W, et al. Cooling precipitation and strengthening study in powder metallurgy superalloy Rene88DT. Mater Sci Eng. A. 2002;332: 318–329.
[22] MatCalc [Internet]. [cited 2018 Jul 6]. Available from: www.matcalc.at.